

A Linear Perturbation Theory of Inhomogeneous Reionization

Jun Zhang^{1*}, Lam Hui¹, Zoltan Haiman²

¹*Department of Physics, Columbia University, 550 West 120th Street, New York, NY 10027, USA*

²*Department of Astronomy, Columbia University, 550 West 120th Street, New York, NY 10027, USA*

10 November 2021

ABSTRACT

We develop an analytic approach to study inhomogeneous reionization on large scales by solving the equations of ionization balance and radiative transfer to first order in perturbations. Given the spatial distribution and spectrum of the ionizing sources, our formalism can be used to predict the large scale power spectra of fluctuations in the abundances of HII, HI and radiation. Our approach avoids common approximations/assumptions in existing analytic methods – for instance, we do not assume a specific ionization topology from the outset; nor do we make a step-function bubble-like approximation to the HII distribution. Applying our formalism to sources biased according to the Press-Schechter prescription, we find: 1. reionization always proceeds “inside-out”, with dense regions more highly ionized, at least on large scales; 2. on sufficiently large scales, HII, HI and radiation exhibits a scale independent bias relative to dark matter; 3. the bias is suppressed on scales comparable to or smaller than the mean free path of the ionizing photons; 4. if the ionizing source spectrum is sufficiently soft, the HII bias closely tracks the source bias for most of the reionization process but drops precipitously after percolation; 5. if the ionizing source spectrum is sufficiently hard, the HII bias drops in a more steady fashion throughout the reionization process. The tools developed here will be useful for interpreting future 21 cm, CMB and Lyman-alpha forest observations, both to learn about the reionization astrophysics (such as the hardness of the source spectrum and therefore the nature of the ionizing sources) and to possibly extract interesting cosmological information.

Key words: cosmology: theory - intergalactic medium - diffuse radiation

1 INTRODUCTION

After the CMB photons decoupled at redshift about 1100, the intergalactic medium (IGM) remained neutral until the first generation of luminous sources produced ionizing photons. Recent measurements of the spectra of high redshift quasars in the Sloan Digital Sky Survey (Becker et al. 2001; White et al. 2003; Fan et al. 2006) and of polarization anisotropies in the cosmic microwave background (CMB) by the *Wilkinson Microwave Anisotropy Probe* (*WMAP*) (Page et al. 2006; Spergel et al. 2006) indicate that the IGM was reionized during redshifts $z \approx 6 - 15$. The history of cosmic reionization contains abundant information about the formation of the first cosmic structures, and can be probed in various future observations, such as redshifted 21cm signatures (Field 1958; Scott & Rees

1990; Madau et al. 1997; Zaldarriaga et al. 2004), the kinetic Sunyaev-Zel’dovich effect (Sunyaev & Zel’dovich 1980; Gruzinov & Hu 1998; Knox et al. 1998; Valageas et al. 2001; Santos et al. 2003; Salvaterra et al. 2005), improved measurements of the large-angle CMB polarization fluctuations (Kaplinghat et al. 2003; Zaldarriaga 1997), the thermal state of the intergalactic medium (Theuns et al. 2002; Hui & Haiman 2003), and Lyman α galaxy populations (Haiman & Spaans 1999; Haiman 2002; Santos et al. 2004; Rhoads & Malhotra 2004; Haiman & Cen 2005). Being directly related to many observables, the distribution of the HI/HII regions during reionization has been studied extensively using both semi-analytic models and hydrodynamic simulations (see, e.g., the recent review by Choudhury & Ferrara (2006), and references therein). If the spectrum of the first ionizing sources is soft (such as a normal stellar spectrum), then the distribution of the ionized regions can be described by discrete HII bubbles around

* E-mail: jz203@columbia.edu

high density regions (Haiman & Loeb 1997). On the other hand, if the source spectrum is hard and extends to X-ray energies (such as for miniquasars), the photons can more readily escape into the IGM, and may ionize the low-density regions first (Miralda-Escudé et al. 2000; Oh 2001; Venkatesan et al. 2001).

The reionization topology in the above two limiting cases are often referred to as “inside-out” and “outside-in” respectively. We will adopt this distinctive terminology here, and we will use it to describe the ionization topology on arbitrarily large scales. Existing analytic/semi-analytic models have generally described either one or the other of these two limiting scenarios (i.e. by following the filling factor of ionized bubbles, or by assuming a uniformly rising ionizing background). The previous methods used to implement such models cannot be easily generalized to derive statistics of the ionization topology, as a continuous function of the hardness of the source spectra. *The goal of the present paper is to construct a model of inhomogeneous reionization in which we can quantify properties of the ionization topology for sources with different spectral hardness and clustering properties. The hope is to derive from first principles, rather than assume, the large scale ionization topology and statistics.* More generally, the nature – the spectrum, spatial clustering, and evolution – of the ionizing source population is poorly known at present, and future observations (as mentioned above) promise to shed much light on these quantities. Parameterized models, such as the one presented here, will be useful for interpreting these future observations.

In principle, hydrodynamic simulations offer an alternative and more reliable way of studying the topology of reionization. However, it is difficult for the state-of-art simulations to cover large scales ($\geq 20\text{Mpc}$) while resolving the sources and the gas distribution on small scales. Recently, several groups have attempted to study the large scale properties of reionization using large scale simulations (Kohler et al. 2005; Iliev et al. 2005; Zahn et al. 2006; Mellema et al. 2006; Iliev et al. 2006). Kohler et al. (2005) for instance adopt a hybrid approach which combines small scale and large scale simulations. As will become clear below, our analytic treatment is in some sense similar: we use linear perturbation theory to address large scale questions while taking into account the effects of small scale clumping in the background evolution. Even if in the future simulations that simultaneously resolve the necessary small scale structure and span over large scales were to become available, we would still need an analytic framework to better understand the physics of reionization. Furthermore, the ionizing sources have to be inserted into the simulations, and their properties specified, essentially by hand. In practice, it is likely that the interpretation of future data on the ionization topology will require an exploration of various parameters of the sources that cannot be computed ab-initio. This, in turn, will require a semi-analytic, computationally less expensive model.

In a hierarchical universe such as our own, one expects linear perturbation theory to work on sufficiently large scales.¹ The spatial fluctuations in the ionized/neutral hy-

drogen and in the ionizing radiation can be related to the dark matter distribution via bias factors which are scale dependent in general. For a given source distribution, these bias factors are determined by the radiative transfer equations and the equation of the photo-ionization balance. The approach followed in this paper is to solve the linearized versions of these equations in Fourier space. Given the source distributions and spectra, this approach allows us to calculate the linear biases of the ionized/neutral hydrogen and of the ionizing radiation, and to follow their evolution. The price paid is that our predictions for the spatial fluctuations are invalid on small scales.

Our calculation takes into account all of the relevant physical processes, including photo-ionization, recombination, the diffusion of photons, the peculiar velocity of the baryons, and the redshifting of photons due to the expansion of the universe. It is worth noting that in the existing semi-analytic models, typically only photo-ionization and recombination are treated in an exact manner². Most of the other processes are either missing or treated approximately. Our formalism accounts for all the relevant processes (albeit in a perturbative manner) and allows a comprehensive study of the dynamical evolution of the HI/HII regions and the radiation field with a general source spectra. It is our hope that the approach taken here can be developed further in future work, and will ultimately make it possible to constrain the high redshift source properties using future 21cm and CMB observations. Our approach is also useful for addressing the question of what robust cosmological information can obtain from future 21cm and CMB observations (for instance, to what extent are the various linear biases scale independent).

The rest of this paper is organized as follows. In §2, we introduce our formalism, and present techniques for solving the equations. In §3, we discuss our assumptions about the ionizing source population, based on the extended Press-Schechter model and assuming different source spectra. In §4, we present our main results, i.e. the evolution of the ionization fluctuations on different scales, and for different source spectra. In §5, we discuss various caveats, and possible extensions of the present paper to future work. Finally, in §6, we summarize our conclusions and the implications of this work. Appendix A presents an analytic solution (up to the numerical solution of a simple integral equation) to the first order radiative transfer and ionization equations. Ap-

the form of HII bubbles. We give some plausibility arguments in Appendix B. Note that exactly the same issue can be raised in the perhaps more familiar context of large scale structure formation – there, it is known that linear perturbation theory works well on large scales, even in the late universe (such as today) when highly nonlinear structures exist on small scales. Why this should be so is not completely understood, but some plausibility arguments were given by Peebles (1980). We borrow his arguments and translate them into the language of reionization, and discuss the conditions (e.g. scales) under which perturbation theory is expected to work, in Appendix B.

² However, we note that Chiu et al. (2003) has a more elaborate model for the evolution of the spatially averaged ionization fraction, but they do not discuss the fluctuations, and/or the dependence of the fluctuations on the source spectrum.

¹ This is by no means obvious, considering the fact that reionization is a messy process on small scales, with large fluctuations in

pendix B contains a preliminary discussion of the validity of linear perturbation theory.

Throughout this paper, we adopt a standard Λ CDM cosmological model, with the parameters $\Omega_m = 0.3$, $\Omega_\Lambda = 0.7$, $\Omega_b = 0.048$, $h = 0.69$, $n = 0.95$, $\sigma_8 = 0.826$, and $\tau = 0.088$, favored by the combination of the three-year WMAP data and the weak lensing data of Canada-France-Hawaii Telescope Legacy Survey (CFHTLS) (see Spergel et al. 2006).

2 THE FORMALISM

We begin with definitions of the physical quantities and descriptions of relevant equations in §2.1. The equations are solved by splitting into two pieces: a spatially averaged piece in §2.2 and a (first order) fluctuating piece in §2.3.

2.1 Definitions and Basic Equations

Let us first define the relevant physical quantities:

$$\begin{aligned} n_{HII} &= n_{HII}(\vec{x}, \tau) \\ n_H &= n_H(\vec{x}, \tau) \\ n_\gamma &= n_\gamma(\vec{x}, \tau, \mu, \vec{\Omega}) \\ S &= S(\vec{x}, \tau, \mu, \vec{\Omega}) \end{aligned} \quad (1)$$

where n_{HII} and n_H are the comoving number densities of the ionized and total hydrogen atoms (ionized+neutral) respectively. They are defined as functions of the comoving coordinate \vec{x} and the conformal time τ . Here, n_γ refers to the comoving photon number density per unit solid angle $d^2\vec{\Omega}$ around the propagation direction $\vec{\Omega}$ and per unit frequency parameter μ . The frequency parameter μ is defined as:

$$\mu = \ln \nu - \ln \nu_0 \quad (2)$$

where ν is the photon frequency, $\nu_0 = 13.6eV/(2\pi\hbar)$ is the ionization threshold of hydrogen, and \hbar is the Planck constant. The frequency parameter will turn out to be more convenient to use than the frequency itself. The quantity $S/4\pi$ is the differential ionizing emissivity, which gives the number of photons emitted by sources per unit comoving volume, per unit conformal time, per unit frequency parameter μ and per unit solid angle.

It is useful to relate n_γ and S here to perhaps more familiar quantities. The proper specific intensity J of the ionizing radiation is related to n_γ via

$$J = \hbar n_\gamma / a^3$$

where a is the scale factor. Note that we set the speed of light to unity throughout this paper. The quantity S is related to the proper emissivity j as usually defined via

$$j = \hbar S / (4\pi a^4)$$

Throughout this paper, for simplicity, we will ignore the presence of helium atoms³. This could affect our results somewhat for the hard-spectrum cases considered below (since most of the > 100 eV photons will be absorbed

³ Note that we do not replace helium with hydrogen i.e. we have $n_H = Y_H * \Omega_b / m_p$, with $Y_H = 0.76$ the hydrogen mass fraction.

by HeI, rather than HI). We postpone the study of helium reionization to future work. Taking into account peculiar velocities, photo-ionization and recombination, the equation for ionization equilibrium is given by

$$\begin{aligned} &\frac{\partial n_{HII}}{\partial \tau} + \vec{\nabla} \cdot (n_{HII} \vec{u}) \\ &= (n_H - n_{HII}) \int_0^\infty d\mu \int d^2\vec{\Omega} n_\gamma \frac{\sigma(\mu)}{a^2(\tau)} \kappa(\mu, \phi) \\ &\quad - \frac{\alpha_B n_{HII}^2}{a^2(\tau)} \end{aligned} \quad (3)$$

where $a(\tau)$ is the cosmological scale factor; \vec{u} is the comoving velocity of the ionized hydrogen atoms; $\sigma(\mu)$ is the photo-ionization cross section (Osterbrock et al. 2005); and $\alpha_B = 2.6 \times 10^{-13} \text{ cm}^3 \text{ s}^{-1}$ is the case B recombination coefficient at temperature equal to 10^4 K .⁴ We have implicitly assumed electric neutrality everywhere in the universe, and we are ignoring the electrons that would result from the ionization of helium, therefore the recombination term is proportional to n_{HII}^2 . The factor $\kappa(\mu, \phi) = 1 + C(\exp(\mu) - 1)(1 - \phi^a)^b$ is included to account for multiple ionizations by an X-ray photon through secondary ionizations by the fast photo-electrons. Here $\phi = n_{HII}/n_H$ is the local ionization fraction, and we adopt the values of $C = 0.3908$, $a = 0.4092$, and $b = 1.7592$ in the fitting formula above (according to Shull & Van Steenberg 1985⁵). The evolution of the radiation background is affected by the sources, the photo-ionization process, the diffusion of photons⁶ and the red-shifting due to the expansion of the universe, all of which are reflected in the following radiative transfer equation (e.g. Gnedin & Ostriker 1997)⁷,

$$\begin{aligned} &\frac{\partial n_\gamma}{\partial \tau} + \vec{\Omega} \cdot \vec{\nabla} n_\gamma - H(\tau) a(\tau) \frac{\partial n_\gamma}{\partial \mu} \\ &= \frac{S}{4\pi} - (n_H - n_{HII}) n_\gamma \frac{\sigma(\mu)}{a^2(\tau)}, \end{aligned} \quad (4)$$

where $H(\tau) = \frac{d \ln a}{d \tau}$ is the Hubble parameter. Our main task is to solve eq.[3] and eq.[4]. For our purpose, it is useful

⁴ The recombination coefficient is weakly temperature dependent. At temperatures T typical of the photoionized intergalactic medium (where recombination is relevant), the recombination coefficient scales roughly as $T^{-0.7}$. The temperature is in turn related to gas density to some power, with the power index ranging from about 0.0 to 0.6 (Hui & Gnedin 1997). Overall, the spatial fluctuation of the recombination coefficient in ionized regions due to the fluctuation in density (and therefore temperature) is rather weak, and is ignored here.

⁵ We caution that the fitting formula only works well for high energy photons ($\gtrsim 1 \text{ keV}$).

⁶ Note that the word ‘‘diffusion’’ refers to the term $\vec{\Omega} \cdot \vec{\nabla} n_\gamma$ in eq.[4], and does not imply scattering. This is a very loose usage because this is not the usual term in the diffusion equation.

⁷ This equation ignores recombination radiation, gravitational redshift and Doppler shift by peculiar motion. Gravitational redshift is a negligible effect except on scales comparable to the horizon. Doppler shift by peculiar motion does not contribute to first order in perturbations (after averaging over the photon directions, which is what we will do eventually); its contribution to second order is negligible compared to other existing second order terms. The importance of recombination radiation is diminished to some extent by the cosmological redshift.

to rewrite the definitions in eq.[1] in terms of the spatial averages and the perturbations:

$$\begin{aligned} n_{HII} &= \bar{n}_H f_{HII}(\tau)[1 + \delta_{HII}(\vec{x}, \tau)] \\ &= \bar{n}_H [f_{HII}(\tau) + \Delta_{HII}(\vec{x}, \tau)] \end{aligned} \quad (5)$$

$$n_H = \bar{n}_H [1 + \delta(\vec{x}, \tau)]$$

$$\begin{aligned} n_\gamma &= \bar{n}_H f_\gamma(\tau, \mu)[1 + \delta_\gamma(\vec{x}, \tau, \mu, \vec{\Omega})] \\ &= \bar{n}_H [f_\gamma(\tau, \mu) + \Delta_\gamma(\vec{x}, \tau, \mu, \vec{\Omega})] \end{aligned}$$

$$\begin{aligned} S &= \bar{n}_H f_s(\tau, \mu)[1 + \delta_s(\vec{x}, \tau, \mu, \vec{\Omega})] \\ &= \bar{n}_H [f_s(\tau, \mu) + \Delta_s(\vec{x}, \tau, \mu, \vec{\Omega})] \end{aligned}$$

where f_{HII} and f_γ are the mean number densities of ionized hydrogen atoms and photons respectively, and f_s is the mean source emissivity – all normalized by the mean co-moving total (i.e. ionized plus neutral) hydrogen number density \bar{n}_H , which is a constant in time. δ , δ_{HII} , δ_γ and δ_s are the corresponding overdensities. Δ_{HII} , Δ_γ and Δ_s are introduced because they greatly simplify the following calculations. We will assume below that the (total) hydrogen fluctuations faithfully trace the dark matter fluctuations (with no bias), which is justified on scales well above the Jeans scale (e.g. Gnedin & Hui 1998). Note that according to the above definitions the neutral hydrogen density is given by

$$n_{HI} = \bar{n}_H [(1 - f_{HII}) + \delta - \Delta_{HII}]$$

and

$$\delta_{HI} = \frac{n_{HI} - \bar{n}_{HI}}{\bar{n}_{HI}} = \frac{\delta - \Delta_{HII}}{1 - f_{HII}} \quad (6)$$

2.2 The Spatial Averages

2.2.1 The Exact Solutions

Taking the spatial (and angular) averages of eq.[3] and eq.[4], we find:

$$\begin{aligned} \frac{\partial f_{HII}}{\partial \tau} &= 4\pi(1 - f_{HII}) \int d\mu \frac{\sigma \bar{n}_H}{a^2} \langle \kappa \rangle f_\gamma C_{\gamma H}^{(1)} \\ &- \frac{\alpha_B \bar{n}_H}{a^2} f_{HII}^2 C_{HII} \end{aligned} \quad (7)$$

$$\begin{aligned} \frac{\partial f_\gamma}{\partial \tau} &= \frac{f_s}{4\pi} + Ha \frac{\partial f_\gamma}{\partial \mu} \\ &- \frac{\sigma \bar{n}_H}{a^2} (1 - f_{HII}) f_\gamma C_{\gamma H}^{(2)} \end{aligned} \quad (8)$$

where $C_{\gamma H}^{(1)}$ and $C_{\gamma H}^{(2)}$ are the clumping factors for photo-ionization, defined as:

$$\begin{aligned} C_{\gamma H}^{(1)} &= \frac{\langle n_{HI} n_\gamma \kappa \rangle}{\langle n_{HI} \rangle \langle n_\gamma \rangle \langle \kappa \rangle} \\ C_{\gamma H}^{(2)} &= \frac{\langle n_{HI} n_\gamma \rangle}{\langle n_{HI} \rangle \langle n_\gamma \rangle} \end{aligned} \quad (9)$$

$C_{HII} = \langle n_{HII}^2 \rangle / \langle n_{HII} \rangle^2$ is the clumping factor for recombination. To solve for f_{HII} and f_γ , one needs to know the evolutions of $C_{\gamma H}^{(1)}$, $C_{\gamma H}^{(2)}$, and C_{HII} . Since the clumping factors are likely dominated by non-linear density variations on small scales (e.g. Haiman, Abel & Madau 2001) their

values cannot be computed reliably in our present framework. We assume, for simplicity, that the clumping factors are known from small scale hydrodynamic simulations. Note that recent large scale radiative transfer simulations effectively adopt the same assumption (e.g. Kohler et al. 2005).

Instead of τ , let us use $\omega = \ln a(\tau)$ as the time variable. To further simplify the notation, we define $\tilde{\sigma}(\tau, \mu) = \sigma(\mu) \bar{n}_H / (Ha^3)$ and $\tilde{\alpha}_B(\tau) = \alpha_B \bar{n}_H / (Ha^3)$, which can be interpreted as follows: $\tilde{\sigma}$ is the probability that a photon of energy μ experiences a direct photo-ionization in Hubble time if the universe is neutral; $\tilde{\alpha}_B$ is the average number of recombinations a proton would experience in a Hubble time if the universe is completely ionized. Eq.[7] and eq.[8] can then be rewritten as:

$$\begin{aligned} \frac{\partial f_{HII}}{\partial \omega} &= 4\pi(1 - f_{HII}) \int_0^\infty d\mu \tilde{\sigma}(\mu) f_\gamma C_{\gamma H}^{(1)} \\ &- \tilde{\alpha}_B f_{HII}^2 C_{HII} \end{aligned} \quad (10)$$

$$\begin{aligned} \frac{\partial f_\gamma}{\partial \omega} &= \frac{f_s}{4\pi Ha} + \frac{\partial f_\gamma}{\partial \mu} \\ &- (1 - f_{HII}) \tilde{\sigma} f_\gamma C_{\gamma H}^{(2)} \end{aligned} \quad (11)$$

Eq.[10] and eq.[11] can be solved iteratively. To do so, we need to use a trick which also appears in §2.3. First, let us change the variables from (ω, μ) to (u, v) which are defined as:

$$\begin{aligned} u &= \frac{1}{2}(\omega + \mu) \\ v &= \frac{1}{2}(\omega - \mu) \end{aligned} \quad (12)$$

Therefore

$$\frac{\partial}{\partial v} = \frac{\partial}{\partial \omega} - \frac{\partial}{\partial \mu} \quad (13)$$

Eq.[11] can be transformed into:

$$\frac{\partial f_\gamma}{\partial v} = \frac{f_s}{4\pi Ha} - (1 - f_{HII}) \tilde{\sigma} f_\gamma C_{\gamma H}^{(2)} \quad (14)$$

or in a simpler form as:

$$\frac{\partial f_\gamma}{\partial v} = q(u, v) - p(u, v) f_\gamma \quad (15)$$

where $q = f_s / (4\pi Ha)$ and $p = (1 - f_{HII}) \tilde{\sigma} C_{\gamma H}^{(2)}$. Eq.[15] is a standard first order differential equation. Its solution reads:

$$f_\gamma(u, v) = \int_{-\infty}^v dv' q(u, v') \exp\left[-\int_{v'}^v dv'' p(u, v'')\right] \quad (16)$$

or in terms of the variables (ω, μ) as:

$$\begin{aligned} f_\gamma(\omega, \mu) &= \int_{-\infty}^\omega d\omega' q(\omega', \mu + \omega - \omega') \\ &\times \exp\left[-\int_{\omega'}^\omega d\omega'' p(\omega'', \mu + \omega - \omega'')\right] \end{aligned} \quad (17)$$

The above solution assumes that there are no ionizing photons at arbitrarily early times and/or arbitrarily high energies.

Using eq.[17], we can obtain $f_\gamma(\omega, \mu)$ for an initial $f_{HII}(\omega)$. f_γ can then be used to calculate a new f_{HII} using eq.[10]. In practice, we find that if this procedure is repeated, f_γ and f_{HII} converge to their true values after around ten iterations.

2.2.2 Useful Approximations

Eq.[17] presents a useful picture of physics: it shows that at the early stage of reionization (when the IGM is not highly ionized), the low energy photons (but above 13.6eV) have a short memory of their past history because they are quickly absorbed by neutral hydrogen. This can be seen from the largeness of the exponent in eq.[17] when the cross section is large. In contrast, the hard photons retain a long memory. Another way of saying the same thing is that the soft photons have a short mean free path compared to the hard photons. This fact leads to a much simpler way of solving eq.[10] and eq.[11] when the average ionized fraction f_{HII} is not close to one. First of all, we notice that in the low energy limit, eq.[17] reduces to a simple form:

$$\begin{aligned} f_\gamma(\omega, \mu) &= q(\omega, \mu)/p(\omega, \mu) \\ &= \frac{f_s}{4\pi(1 - f_{HII})Ha\tilde{\sigma}C_{\gamma H}^{(2)}} \end{aligned} \quad (18)$$

Secondly, we assume there is a critical frequency parameter μ_c , above which the photons hardly ionize any neutral hydrogen during reionization, and below which eq.[18] is valid. Therefore, eq.[10] can be rewritten as:

$$\begin{aligned} \frac{\partial f_{HII}}{\partial \omega} &= \frac{1}{Ha} \int_0^{\mu_c} d\mu f_s(\omega, \mu) \langle \kappa \rangle C_{\gamma H}^{(1)}/C_{\gamma H}^{(2)} \\ &- \tilde{\alpha}_B C_{HII} f_{HII}^2 \end{aligned} \quad (19)$$

Eq. [18] essentially describes an emission-absorption equilibrium, i.e. all emitted photons with $0 < \mu < \mu_c$ are consumed by ionization. It should be noted that if the source spectrum is hard (*i.e.* high percentage of photo-ionization is caused by high energy photons.), Eq. [18] and [19] are not a good approximation anymore. This will be discussed further in §2.3 and §4. Note that throughout this paper, we compute the exact solutions rather than employ the approximations outlined above, though we will compare the two in §4.

2.3 The Linear Perturbations

2.3.1 The Exact Solutions

Let us denote the Fourier transforms of δ , Δ_s , Δ_{HII} and Δ_γ as $\tilde{\delta}$, $\tilde{\Delta}_s$, $\tilde{\Delta}_{HII}$ and $\tilde{\Delta}_\gamma$ respectively. The Fourier transforms of eq.[3] and eq.[4] to the first order⁸ are:

$$\frac{\partial \tilde{\Delta}_{HII}}{\partial \omega} = G\tilde{\delta} - F\tilde{\Delta}_{HII} + \int_0^\infty d\mu \langle \kappa \rangle \int d^2\vec{\Omega} \tilde{\Delta}_\gamma B \quad (20)$$

$$\frac{\partial \tilde{\Delta}_\gamma}{\partial \omega} = \frac{\partial \tilde{\Delta}_\gamma}{\partial \mu} - M\tilde{\Delta}_\gamma + N\tilde{\Delta}_s + R(\tilde{\Delta}_{HII} - \tilde{\delta}) \quad (21)$$

where

$$\begin{aligned} F &= 2\tilde{\alpha}_B f_{HII} \\ &+ 4\pi \int_0^\infty d\mu \tilde{\sigma} f_\gamma \left[\langle \kappa \rangle - (1 - f_{HII}) \frac{\partial \kappa}{\partial \phi} \Big|_{\phi=f_{HII}} \right] \\ G &= \frac{d \ln D}{d\omega} f_{HII} \end{aligned} \quad (22)$$

⁸ The question of whether/when retaining only first order perturbations is justified is discussed below and in Appendix B.

$$\begin{aligned} &+ 4\pi \int_0^\infty d\mu \tilde{\sigma} f_\gamma \left[\langle \kappa \rangle - (1 - f_{HII}) f_{HII} \frac{\partial \kappa}{\partial \phi} \Big|_{\phi=f_{HII}} \right] \\ B &= (1 - f_{HII}) \tilde{\sigma} \\ M &= (1 - f_{HII}) \tilde{\sigma} - \frac{i\vec{k} \cdot \vec{\Omega}}{Ha} \\ N &= (4\pi Ha)^{-1} \\ R &= \tilde{\sigma} f_\gamma \end{aligned}$$

and \vec{k} is the wave vector.⁹ For simplicity, we do not show the k dependence explicitly for the Fourier modes. In deriving eq.[20], we have used the fact that to the first order, on large scales, the dark matter overdensity grows linearly with a growth factor defined by $D(\tau)$, and the peculiar velocity is proportional to the gradient of the gravitational potential. The great advantage of the Fourier transformation is that it allows us to solve eq.[21] using tricks similar to those introduced in the previous section, *i.e.* :

$$\begin{aligned} \tilde{\Delta}_\gamma(\omega, \mu, \vec{\Omega}) &= \int_{-\infty}^\omega d\omega' \{ N(\omega') \tilde{\Delta}_s(\omega', \mu + \omega - \omega', \vec{\Omega}) \\ &+ R(\omega', \mu + \omega - \omega') [\tilde{\Delta}_{HII}(\omega') - \tilde{\delta}(\omega')] \} \\ &\times \exp[- \int_{\omega'}^\omega d\omega'' M(\omega'', \mu + \omega - \omega'', \vec{\Omega})] \end{aligned} \quad (23)$$

The first line above describes the contributions to fluctuations in radiation from fluctuations in the spatial distribution of the ionizing sources; the second line describes the contributions from fluctuations in absorbers; the third line accounts for the modulation by optical depth, *i.e.* it tells us the distance to which one needs to integrate. By integrating eq.[23] over $\vec{\Omega}$, one can obtain the monopole perturbation of the radiation field, which is what is needed in eq.[20]:

$$\begin{aligned} &\int d^2\vec{\Omega} \tilde{\Delta}_\gamma(\omega, \mu, \vec{\Omega}) \\ &= 4\pi \int_{-\infty}^\omega d\omega' \{ N(\omega') \tilde{\Delta}_s(\omega', \mu + \omega - \omega') \\ &+ R(\omega', \mu + \omega - \omega') [\tilde{\Delta}_{HII}(\omega') - \tilde{\delta}(\omega')] \} \\ &\times \exp[- \int_{\omega'}^\omega d\omega'' B(\omega'', \mu + \omega - \omega'')] \\ &\times \frac{\sin[P(\omega, \omega')k]}{P(\omega, \omega')k} \end{aligned} \quad (24)$$

where

$$P(\omega, \omega') = \int_{\omega'}^\omega d\omega'' \frac{1}{H(\omega'')a(\omega'')} \quad (25)$$

In writing down the above expression, we have assumed that the dominant contribution is from the monopole of $\tilde{\Delta}_s$ (note that we have dropped the argument $\vec{\Omega}$ to signify the fact that this is the monopole component). Note that we are *not* assuming $\tilde{\Delta}_\gamma$ has no higher multipoles; rather, we are assuming that, as far as the source contribution is concerned, the monopole of $\tilde{\Delta}_\gamma$ is dominated by the monopole of the source emissivity. This assumption can be motivated in two different ways. First, in the low k limit (which is the regime where perturbation theory probably works best), one can show that the monopole dominates. Second, on large

⁹ Throughout this paper, we approximate $\langle \kappa(\mu, \phi) \rangle$ by $\kappa(\mu, \langle \phi \rangle)$.

scales, since one is averaging over many sources, the resulting smoothed emissivity is probably close to isotropic even if the individual sources are not.

Eq. [24], together with eq. [20], allows for an iterative solution for $\tilde{\Delta}_{HII}$ and $\tilde{\Delta}_\gamma$ given the source distribution $\tilde{\Delta}_s$ and the dark matter overdensity $\tilde{\delta}$. In Appendix A, we present a further improved scheme of finding the numerical solution.

2.3.2 Useful Approximations

Similar to what we have done in §2.2, when the universe is not close to being fully ionized, eq.[24] for soft photons can be greatly simplified. First, we notice that the factor $\sin[P(\omega, \omega')k]/[P(\omega, \omega')k]$ in eq.[24] should be very close to unity for soft photons. There are two reasons for this: one is because the wave number k of interest is small; the other reason is that the large exponent B limits the magnitude of $\omega - \omega'$ to be very small in the integration. Taking these into account, eq.[24] becomes much simpler:

$$\int d^2\tilde{\Omega}\tilde{\Delta}_\gamma(\omega, \mu < \mu_c, \tilde{\Omega}) \quad (26)$$

$$= \frac{4\pi}{B(\omega, \mu)} \{N(\omega)\tilde{\Delta}_s(\omega, \mu) + R(\omega, \mu)[\tilde{\Delta}_{HII}(\omega) - \tilde{\delta}(\omega)]\}$$

The above expression is the analog of eq. [18], representing essentially emission-absorption equilibrium. Using the same critical frequency parameter μ_c to isolate the contributions from the soft photons as in eq.[19], and assuming eq.[26] is correct for such soft photons, we obtain:

$$\frac{\partial\tilde{\Delta}_{HII}}{\partial\omega} = \left(\frac{d\ln D}{d\omega} - Y\right) f_{HII}\tilde{\delta} \quad (27)$$

$$- (2\tilde{\alpha}_B f_{HII} - Y)\tilde{\Delta}_{HII}$$

$$+ \frac{1}{Ha} \int_0^{\mu_c} d\mu \langle \kappa \rangle \tilde{\Delta}_s(\omega, \mu)$$

where

$$Y = 4\pi(1 - f_{HII}) \int_0^\infty d\mu \tilde{\sigma} f_\gamma \left. \frac{\partial\kappa}{\partial\phi} \right|_{\phi=f_{HII}} \quad (28)$$

Again, eq.[27] is a good approximation when the source spectrum is not too hard. In §4, we quantify this statement and discuss the choice of μ_c with realistic examples. We reiterate that all of our conclusions in this paper are based on the exact solutions rather than the approximations outlined above, though we do compare the two in §4.

At this point, the reader might wonder: since reionization is likely a complicated process with large fluctuations on small scales, could these fluctuations invalidate linear perturbation theory on large scales? In other words, how should one justify the use of perturbation theory on large scales? This is actually a difficult question. The same question arises in the context of large scale structure formation: how do we justify the use of linear perturbation theory on large scales today, knowing that there are highly nonlinear structures on small scales, such as galaxies, clusters and so on? Some plausibility arguments exist (Peebles 1980), and we will discuss the analogs of these arguments for reionization in Appendix B. However, the only rigorous method of validation that we know of is to appeal to numerical simulations. We will perform comparisons of our calculations with numerical radiative transfer simulations in another paper.

At least one difference between reionization and large scale structure is, however, worth emphasizing. In the case of reionization, the spatial averages are undoubtedly affected by small scale clumping – hence the need to introduce clumping factors in eq. [7] and [8]. In some sense, our treatment here is quite similar to some of the recent numerical simulations (Kohler et al. 2005) which incorporate small scale clumping by hand while focusing on the large scale fluctuations. In the case of large scale structure, the spatially averaged equations are those that govern the global expansion of the universe i.e. the Friedmann equation and energy-momentum conservation. In that case, small scale clumping appears not to affect significantly the evolution of the spatial averages (e.g. Hui & Seljak 1996; see however Kolb et al. 2005 for a different view).

3 MODELING THE IONIZING SOURCE POPULATION

Solving the equations described in the previous section requires specifying the source properties, including the emissivity as a function of redshift, and the spatial distribution and spectrum of the ionizing sources. In this paper, we use the extended Press-Schechter theory (Press & Schechter 1974; Bond et al. 1991; Lacey & Cole 1993) to model the abundance and spatial distribution of the ionizing sources. It is important to emphasize that this is for illustration only – our formalism as laid out in the previous section is certainly not wedded to this particular model of the ionizing source population.

3.1 Dark Matter Halo Abundance

The minimum halo that can host luminous sources should have a virial temperature above 10^4K to allow efficient hydrogen line cooling (see, *e.g.* Mesinger et al. 2006). This leads to a minimum halo mass given by:

$$M_{min} \approx 1.3 \times 10^7 M_\odot \left(\frac{T_{vir}}{10^4\text{K}}\right)^{3/2} \left(\frac{1+z}{21}\right)^{-3/2} \quad (29)$$

$$\times \left(\frac{\Omega_m}{0.3}\right)^{-1/2} \left(\frac{h}{0.7}\right)^{-1} \left(\frac{\mu_{mol}}{1.22}\right)^{-3/2}$$

where μ_{mol} is the mean molecular weight, which is chosen to be 0.6 (appropriate for the ionized gas in halos with a virial temperature above 10^4K) in the following calculations. According to the extended Press-Schechter Model, on mass scale m , the fraction of mass collapsed in halos with masses larger than M_{min} is:

$$f_m^{coll}(\vec{x}, \tau) = \text{erfc} \left[\frac{\delta_c - \delta_m(\vec{x}, \tau)}{\sqrt{2[\sigma_{min}^2(\tau) - \sigma_m^2(\tau)]}} \right] \quad (30)$$

where δ_c is the critical overdensity in the spherical collapse model; δ_m and σ_m^2 are the overdensity and the variance of the density fluctuations on mass scale m respectively; σ_{min}^2 is the density variance corresponding to the mass scale M_{min} . On large scales, σ_m^2 is much smaller than σ_{min}^2 and therefore neglected in the following calculations.

Assuming on average each hydrogen atom in the collapsed objects emits $\gamma(\mu)$ ionizing photons per unit fre-

quency parameter μ , the emissivity function smoothed over scale m is given by:

$$S_m(\vec{x}, \tau, \mu) = \gamma(\mu) \bar{n}_H \frac{\partial}{\partial \tau} [f_m^{\text{coll}}(\vec{x}, \tau)(1 + \delta_m(\vec{x}, \tau))] \quad (31)$$

The factor $1 + \delta_m$ takes into account the mass overdensity. This equation also implicitly assumes that the collapsed objects produce their photon output on a time-scale much shorter than $f^{\text{coll}}/[df^{\text{coll}}/dt]$ (which is justified for short-lived, massive stars, or efficiently accreting black holes). If we choose the scale m to be very large (*e.g.* the horizon size), δ_m can be neglected, and from eq.[31] we obtain the spatially averaged emissivity function defined in §2 as:

$$f_s(\tau, \mu) = \gamma(\mu) \frac{2}{\sqrt{\pi}} \exp\left(-\frac{\delta_c^2}{2\sigma_{\text{min}}^2}\right) \frac{d}{d\tau} \left(\frac{-\delta_c}{\sqrt{2\sigma_{\text{min}}^2}}\right) \quad (32)$$

By Taylor expanding eq.[31] around $\delta_m = 0$ and then performing a Fourier transformation, we obtain the spatial fluctuation of the emissivity as ¹⁰:

$$\begin{aligned} \tilde{\Delta}_s(\vec{k}, \tau, \mu) &= \gamma(\mu) \frac{\partial}{\partial \tau} [R(\tau) \tilde{\delta}(\vec{k}, \tau)] \\ &= \gamma(\mu) \frac{\tilde{\delta}(\vec{k}, \tau)}{D(\tau)} \frac{\partial}{\partial \tau} [R(\tau) D(\tau)] \end{aligned} \quad (33)$$

where

$$R(\tau) = \text{erfc}\left(\frac{\delta_c}{\sqrt{2\sigma_{\text{min}}^2}}\right) + \sqrt{\frac{2}{\pi\sigma_{\text{min}}^2}} \exp\left(-\frac{\delta_c^2}{2\sigma_{\text{min}}^2}\right) \quad (34)$$

and $D(\tau)$ is the linear growth factor.

In our model, we do not take into account the feedback effects discussed in recent papers (Cole et al. 2000; Oh 2001; Benson et al. 2002; Oh & Haiman 2003; Dijkstra et al. 2004; Benson et al. 2005; Kramer et al. 2006; Mesinger et al. 2006, also see Haiman & Holder 2003 for a general reference for feedback effects during reionization). For example, the ionized regions usually have relatively higher temperatures due to photo-heating, leading to a larger filtering scale (Gnedin & Hui 1998) that suppresses the formation of small scale structures. This reduces the clumping factor and hence the recombination rate, and also results in an anti-correlation between the source overdensity and the local ionized fraction. In principle, such a feedback effect can be included in the linear perturbation calculation by inserting into eq. [33] a term that is proportional to $\tilde{\Delta}_{HII}$. We leave a more careful study of such effects to the future.

In our calculation, the normalization of the source emissivity is chosen to give a mean optical depth of Thomson scattering equal to 0.088, which is suggested by the three-year WMAP data. The remaining freedom is to choose the source spectrum, which depends on the type of sources (see, *e.g.*, Oh 2001). Rather than exhausting spectra of general shapes, we focus on spectra of power-law forms with different spectral indices, which cover the possible range of effective spectra of stars and miniquasars. A power-law form in the frequency ν is an exponential form in the frequency parameter μ , *i.e.* :

$$\gamma(\mu) d\mu = \frac{\zeta}{C_\beta} \exp[(\beta + 1)\mu] d\mu \quad (35)$$

where β is the spectral index, C_β is a normalization factor, and ζ is the total number of ionizing photons generated per baryon in stars, and managing to escape into the IGM. For example, if 10 percent of the baryons turn into stars with a normal Salpeter mass function, and 10 percent of their ionizing radiation escapes, then $\zeta = 40$. The spectrum is smoothly cut off at $\mu = 10$ (~ 300 keV) to allow for a proper normalization even when $\beta \geq -1$. The cutoff does not introduce any artificial effects because the mean free path of photons at this energy greatly exceeds the Hubble distance.

It is worth noting that in a more complicated scenario, the shape of the source spectrum may vary with redshift. For example, if quasars are the dominant ionizing sources at high redshifts ($z \sim 15$), and followed by stars at $z \sim 6$, the hardness of the source spectrum varies with time. Such a case will be studied in a future paper.

4 RESULTS

As we have discussed in §2.2, the spatial averages of the ionized fraction and the radiation intensity can be calculated by solving eq.[10] and eq.[8] once the clumping factors $C_{\gamma H}^{(1)}$, $C_{\gamma H}^{(2)}$, and C_{HII} are provided. According to the existing hydrodynamic simulations, C_{HII} is around order of ten during reionization for a UV dominated source spectrum, but can be less than one for a harder source spectrum¹¹. The values of $C_{\gamma H}^{(1)}$ and $C_{\gamma H}^{(2)}$ vary with both the redshift and the photon energy, but are rarely far from unity (Kohler et al. 2005). For simplicity, in this paper, we choose $C_{HII} = 10$ for $\beta = -3$ or $\beta = -2$, $C_{HII} = 1$ for $\beta = -1$, and $C_{\gamma H}^{(1)} = C_{\gamma H}^{(2)} = 1$ for all cases. We caution that the precise values of the clumping factors are rather uncertain. The important point to keep in mind is that the clumping factors show up explicitly only in the equations for the spatial averages but not for the fluctuations. In other words, they affect the linear perturbations only indirectly through their effects on the background (*i.e.* f_{HII} and f_γ). Once the background is specified, our predictions for the linear perturbations are quite robust. This is discussed further in §5 below.

To illustrate the results, we choose three types of source spectra: ($\zeta = 82, \beta = -3$), ($\zeta = 75, \beta = -2$) and ($\zeta = 50, \beta = -1$). We show the evolution of the spatially averaged ionization fraction f_{HII} in Fig. 1, the HII bias (*i.e.* $\tilde{\delta}_{HII}(\vec{k})/\tilde{\delta}(\vec{k})$) at $k = 0.01 \text{ Mpc}^{-1}$ in Fig. 2, and the HII bias as a function of the scale k at redshift $z = 20, 13, 10, 9$ in Fig. 3. From Fig. 2, we see that in the case of a soft source spectrum (*i.e.* $\beta = -3$ and $\beta = -2$), the bias of the HII regions remains at a high value during most time of reionization, and quickly drops to one when the HII regions percolate the IGM. This can be understood in the usual bubble picture, in which the HII regions are confined within the HII bubbles due to the short mean free path of the photons. Therefore,

¹⁰ Note that the wave mode of the Fourier transformation already indicates a smoothing scale, therefore the scale index m is dropped.

¹¹ Note that the last statement is probably not true at the end of reionization when even high density regions are ionized and $C_{HII} \gg 1$. For simplicity, we ignore the time dependence of the clumping factors in this paper.

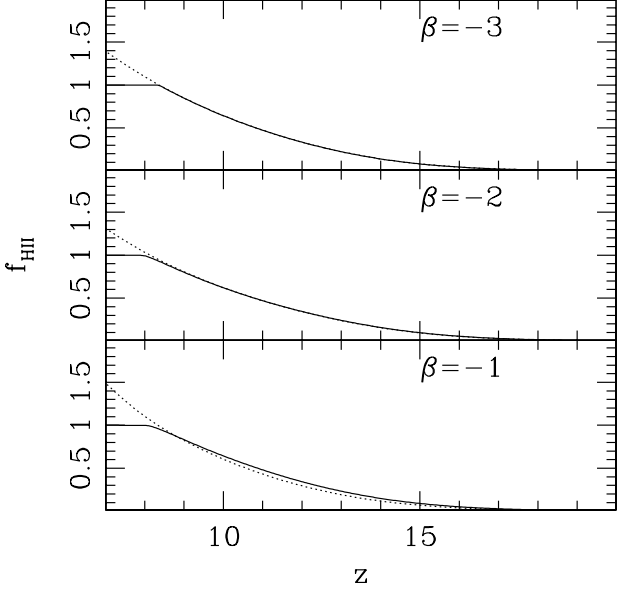


Figure 1. The solid curves show the evolution of the ionized fraction f_{HII} ; the dotted curve is the approximate solution for f_{HII} from eq.[19]. The three panels assume different power law slopes (β) for the source spectrum, as labeled.

the HII regions do not merge on large scales until the mean ionization fraction of the IGM reaches a very high level. In contrast, for a harder source spectrum, the bias of the HII regions decreases in a more continuous fashion. Interestingly, this is not only because hard photons have a much longer mean free path, but also due to the fact that secondary ionizations are more intense in less ionized regions.

The HII bias is intimately related to the issue of inside-out versus outside-in ionization. A reasonable definition of inside-out ionization is that $\langle \delta \delta_X \rangle > 0$, where δ_X is the fluctuation in the ionized fraction. A positive correlation means higher density regions exhibit a higher ionized fraction. Conversely, a negative correlation can be taken as the definition of outside-in ionization. To the lowest order, $\langle \delta \delta_X \rangle = \langle \delta(\delta_{HII} - \delta) \rangle$. Therefore, the sign of $\langle \delta \delta_X \rangle$ is determined by whether the HII bias is greater or less than unity. It is worth noting that whether reionization is inside-out or outside-in can be a scale dependent question: the sign of $\langle \delta \delta_X \rangle$ could depend on the scale of interest (think of δ and δ_X as quantities smoothed on some scale, or think of their Fourier counterparts).

An important feature we learn from Fig. 2 is that the large scale bias of the HII regions is larger than unity in all three cases, which therefore means the high density regions tend to be more ionized than the low density regions. This fact shows that at least on large scales, the topology of the HII regions is inside-out, even for a hard source spectrum. This seems to hold on all scales that we have examined (see Fig. 3), although one must note that our perturbative approach is expected to break down on sufficiently small scales.

By choosing $\mu_c = 3.75$ ($E_\nu \sim 580\text{eV}$), we find that eq.[19] and eq.[27] are good approximations for f_{HII} and $\tilde{\delta}_{HII}$ on large scales (*e.g.* $k \lesssim 0.01 \text{ Mpc}^{-1}$) during most of

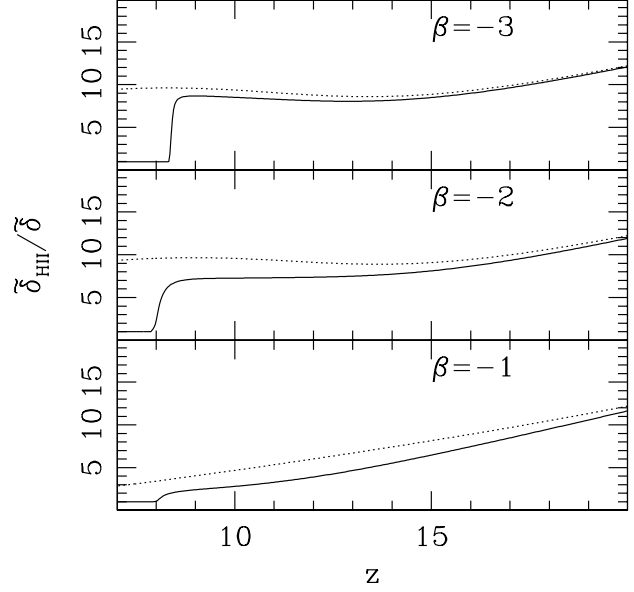


Figure 2. The solid curves show the bias factors of the HII regions at $k = 0.01 \text{ Mpc}^{-1}$; the dotted curves show the approximate solution from eq.[27]. $\tilde{\delta}_{HII}$ and $\tilde{\delta}$ represent the Fourier transforms of the overdensities δ_{HII} and δ , defined in eq.[5].

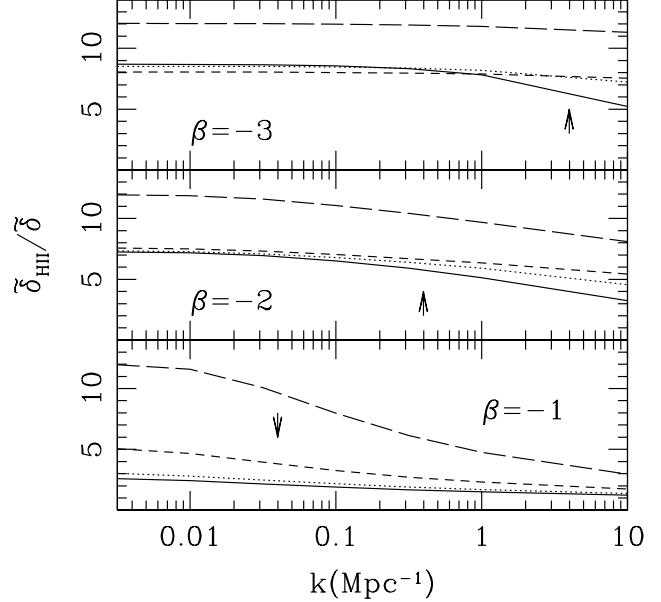


Figure 3. The HII bias as a function of scale. The long dashed, short dashed, dotted, and solid curves are for redshift $z = 20, 13, 10,$ and 9 respectively. The arrows indicate the mean free path of the typical ionizing photon in each case at $z = 9$ (see eq.[37]). We caution that our linear theory becomes inaccurate on small scales ($k \gtrsim 0.1 \text{ Mpc}^{-1}$).

the reionization process for the $\beta = -3$ and $\beta = -2$ cases, as shown in Fig. 1 and Fig. 2. The reason for choosing this value of μ_c is not only that it provides a good fit for both f_{HII} and $\tilde{\delta}_{\text{HII}}$, but also because 580eV corresponds to a critical energy threshold, below which photons are significantly absorbed by neutral hydrogen, as shown in Fig. 5¹². In other words, eq. [18] works well for photons with energies below 580eV during the early stages of reionization. For smaller scales, the agreement becomes worse because the photon propagation suppresses the small scale fluctuations, thus reducing the amplitude of the (HII to dark matter/baryon) bias. This is shown in Fig. 3.

A useful way to see why the bias of HII decays faster for a harder source spectrum is to calculate the mean free path of the ionizing photons. For a specific frequency parameter μ , the comoving mean free path is simply $a^2/[\bar{n}_H\sigma(\mu)(1 - f_{\text{HII}})]$. The average mean free path can be defined as:

$$\lambda = \left[\frac{\bar{n}_H(1 - f_{\text{HII}}) \int_0^{\mu_c} f_\gamma \sigma(\mu)}{a^2 \int_0^{\mu_c} f_\gamma} \right]^{-1} \quad (36)$$

Using eq.[18] for three different source spectral indices, we find:

$$\lambda(\beta = -3) \approx 0.4 \left(\frac{11}{1+z} \right)^2 \left(\frac{0.5}{1 - f_{\text{HII}}} \right) \text{Mpc} \quad (37)$$

$$\lambda(\beta = -2) \approx 5 \left(\frac{11}{1+z} \right)^2 \left(\frac{0.5}{1 - f_{\text{HII}}} \right) \text{Mpc}$$

$$\lambda(\beta = -1) \approx 40 \left(\frac{11}{1+z} \right)^2 \left(\frac{0.5}{1 - f_{\text{HII}}} \right) \text{Mpc}$$

These numbers basically answer the question of why in Fig. 2 the HII bias in the $\beta = -3$ or $\beta = -2$ case does not drop until the ionization fraction is very close to one. This is because in both cases the wave length of $k = 0.01 \text{Mpc}^{-1}$ is larger than the average photon mean free path during most time of reionization. Radiative transfer is unable to suppress perturbations on scales larger than the mean free path, and the HII bias more or less tracks the source bias. In contrast, HII perturbations on smaller scales are more easily suppressed by the radiation, which can be seen in Fig. 3 as the suppression in $\tilde{\delta}_{\text{HII}}/\tilde{\delta}$ for $k \geq 2\pi/\lambda$. However, we caution that our linear theory becomes inaccurate on small scales. We also find that other ways of estimating the average photon mean free path only change the results by a factor of a few, meaning that eq.[36] provides a robust order of magnitude estimate. For example, if secondary ionization is included in eq.[36], the average mean free path in all three cases is increased by no more than a factor of two.

In Fig. 4, we show the redshift dependence of the fluctuation of the neutral fraction with respect to the dark matter (*i.e.* $(1 - f_{\text{HII}})\tilde{\delta}_{\text{HI}}/\tilde{\delta}$) at $k = 0.01 \text{Mpc}^{-1}$, which is proportional to the 21cm signal from the neutral hydrogen (see *e.g.* Zaldarriaga et al. 2004; Zahn et al. 2006). At the early epoch of reionization, this quantity is close to unity since most of the IGM is still neutral. The non-monotonic behavior at lower redshifts may suggest a best window for detect-

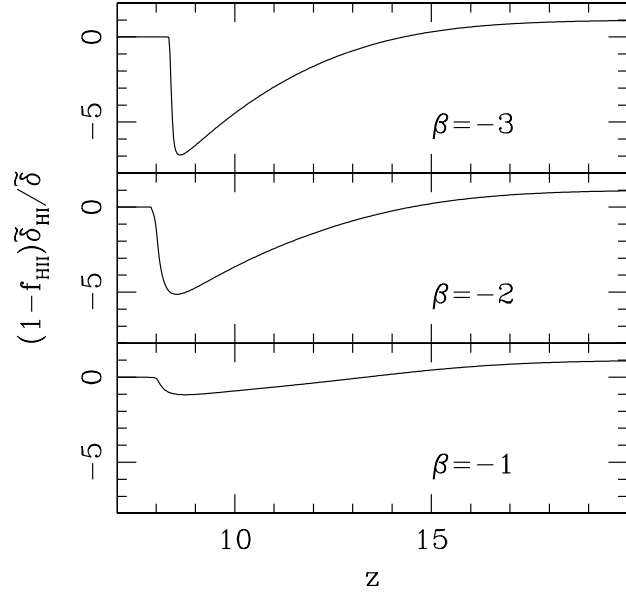


Figure 4. The redshift dependence of $(1 - f_{\text{HII}})\tilde{\delta}_{\text{HI}}/\tilde{\delta}$ at $k = 0.01 \text{Mpc}^{-1}$.

ing the 21cm emission. Such a feature is more pronounced when the source spectrum is soft.

The bias of the radiation monopole ($\int d^2\tilde{\Omega}\tilde{\delta}_\gamma/(4\pi\tilde{\delta})$, which is simply called $\tilde{\delta}_\gamma/\tilde{\delta}$ in the figures) on scales of $k = 0.01 \text{Mpc}^{-1}$ and $k = 0.1 \text{Mpc}^{-1}$ is shown in Fig. 6 as a function of the photon energy for different redshifts, and in Fig. 7 as a function of redshift for different photon energies¹³. Again, one can see a clear difference between the soft and the hard photons, which are divided by the critical line at $E_\nu \sim 580\text{eV}$. The bias of the soft photons remains high until the HII percolation, following closely the bias of HII itself, at least during the early stages of reionization. On the other hand, the high energy photons diffuse relatively freely into the space, leading to an ever decreasing bias.

An interesting feature in Fig. 7 deserves a brief discussion: the bias of the radiation field (especially for soft photons) shoots up quickly right before percolation. In Fig. 2, we notice that for a soft source spectrum, the bias of HII also rises before the time of percolation (but less dramatically). This appears counter-intuitive: naively, one expects that both the HII abundance and the radiation roughly trace the ionizing sources, whose bias in our version of the extended Press-Schechter model always decays with time (shown in Fig. 8). While this intuition is correct in the early stages of reionization, the situation starts to change when the mean ionization fraction becomes significant. This is because a high density region generates more photons than it can consume (by ionization when the ionized fraction is already high), and this leads to run-away, causing the abrupt rise of the bias of the radiation field (with a corresponding,

¹² Note that the y-axis in Fig. 5 is in logarithmic scale. We do not show labels on the y-axis because they are not important for our purpose.

¹³ Unlike the HII bias, the radiation bias is probably unobservable. We plot it here simply for a better understanding of the physics of reionization.

but less dramatic, rise of the HII bias). After percolation, the radiation bias of course drops precipitously because the photons are free to diffuse to large distances. This effect is less pronounced for hard photons because percolation for hard photons is a more gradual process to begin with.

Another interesting feature in Fig. 7 is that the bias of the soft photons exhibits damped oscillations after reionization is complete. This behavior can be traced back to the oscillatory kernel eq.[24]. In the case of $\beta = -3$, the bias of the soft photons right before the percolation of HII bubbles rises up to a high value, meaning that high density regions contain many more photons than low density regions. Such a difference between the high and the low density regions quickly decays away when the HII bubbles merge, *i.e.* when the soft photons are “released” and can freely travel to the neighbouring low density regions. The relaxation of this process leads directly to the oscillations we see in Fig. 7. The oscillations are most pronounced when the wavelength is small (high k) and when the post-percolation drop in bias is most abrupt (*i.e.* when the photons are soft). Note that these oscillations can be washed out by the stochastic bias of the ionizing sources, which is not considered in this paper.

Finally, we find that the biases of both HII/HI and the radiation field remain scale invariant on large scales ($k \leq 0.01 \text{ Mpc}^{-1}$). This is not only because the source bias is scale invariant in our model, but also due to the fact that the diffusion of photons is negligible when the scale of interest is much larger than the mean free path. Using eq.[24] again, we can see that at small k the oscillatory kernel remains constant, therefore the k dependence is essentially removed. The scale invariant nature of the large scale HII/HI bias can be very useful, because it makes it possible to measure the shape of the primordial mass power spectrum using the HI power spectrum. The evolution of the HI fluctuation shown in Fig. 4 may be useful for this purpose in future 21cm observations.

5 DISCUSSION

In this section, we briefly discuss several interesting issues related to our results above. First, recall that the clumping factors $C_{\gamma H}^{(1,2)}$ and C_{HII} are set by hand in our calculations. In particular, we have neglected their dependence on redshift and frequency (the latter is relevant for $C_{\gamma H}^{(1,2)}$). The precise dependence is uncertain, and is only partially addressed by the most recent simulations (see *e.g.* Iliev et al. 2005; Kohler et al. 2005). However, as emphasized before, the clumping factors appear explicitly only in the evolution equations for the spatially averaged quantities (eq. [7] & [8]), and not in the equations for the first order perturbations (eq. [20] & [21]). The clumping factors only influence the first order perturbations indirectly through their influence on the background quantities f_{HII} and f_{γ} . While quantitative details regarding the perturbations do depend on the precise values of the clumping factors, the overall qualitative behavior, such as the evolution of the various biases, remain quite robust.

Another issue concerns the topology of the HII distribution. It is interesting to ask if the topology is still inside-out if the source spectrum is made up of only hard photons. This, for example, is relevant to the scenario proposed by Ricotti

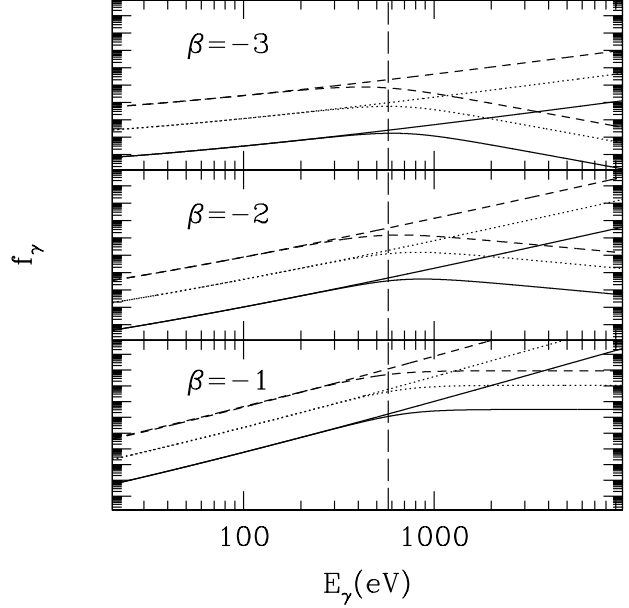


Figure 5. The spectrum of the ionizing background. The vertical line refers to $E_{\gamma} = 580 \text{ eV}$. The solid, dotted and dashed curves are for $z = 18.7$, $z = 13.6$ and $z = 9.8$ respectively. The bended curves are the exact solutions from eq.[11], the straight lines are the approximated solutions from eq.[18].

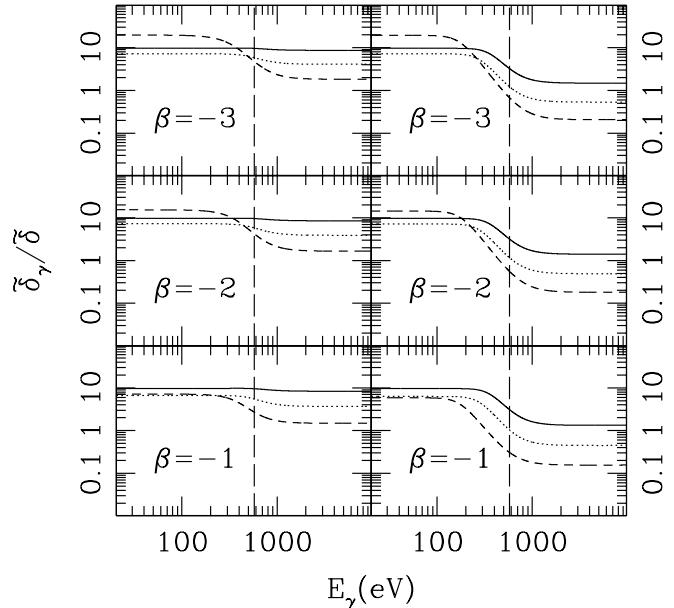


Figure 6. The bias in the ionizing background photon density as a function of photon energy. The vertical long dashed line refers to $E_{\gamma} = 580 \text{ eV}$. The solid, dotted and dashed curves are for $z = 18.7$, $z = 13.6$ and $z = 9.8$ respectively. The left column is for $k = 0.01 \text{ Mpc}^{-1}$, and the right column is for $k = 0.1 \text{ Mpc}^{-1}$.

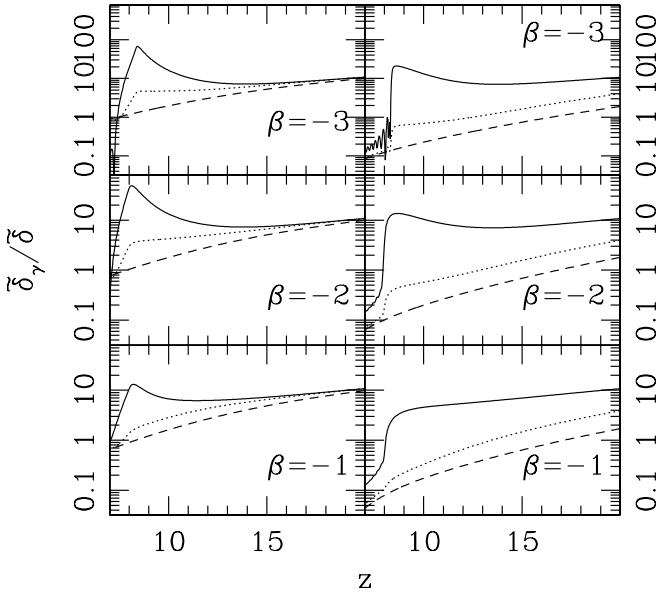


Figure 7. The bias in the ionizing background photon density as a function of redshift. The solid, dotted and dashed curves are for $E_\gamma = 170$ eV, $E_\gamma = 580$ eV and $E_\gamma = 25$ keV respectively. The left column is for $k = 0.01$ Mpc $^{-1}$, and the right column is for $k = 0.1$ Mpc $^{-1}$.

& Ostriker (2004), in which reionization at high redshift is caused by highly obscured miniquasars. To answer this question, we consider three cases, in which we remove the soft photons by mutilating the $\beta = -1$ spectrum and erasing all photons below 170eV, 270eV, 450eV, respectively (the emissivity factor ζ is raised to 80, 100, and 150, respectively to yield the same optical depth). In Fig. 9, we see that the bias of HII always exceeds unity, meaning the topology is not outside-in, but the HII bias does decrease with increasing hardness of the ionizing photons. One can also try to reduce the HII bias by lowering the source bias. In Fig. 10, we repeat the calculation for the case of ($\zeta = 82, \beta = -3$) except that the source bias is artificially set to unity, which is probably the lowest value one can expect, in any scenario in which the ionizing sources populate collapsed halos. We find that the bias of HII is again always larger than one¹⁴. For $\beta = -2$ or $\beta = -1$, the evolution of the HII bias becomes more featureless and very close to unity at all redshifts¹⁵. Therefore, our conclusion about the topology of the HII distribution is robust¹⁶.

¹⁴ Note that the bump at $z \sim 10$ is due to the run-away effect introduced in §4.

¹⁵ In the case of $\beta = -1$ and a source bias of unity, the HII bias right before the end of reionization does go slightly below unity. This means that the ionization topology is marginally outside-in.

¹⁶ We caution that our conclusion is based on the linear perturbation calculation, which does not take into account the spatial fluctuations of the second or higher order terms in the equations. The non-linear opacity and recombination fluctuations are important in determining the shapes and the topology of the HII regions on small scales (< 1 Mpc) (see, *e.g.*, Ciardi et al. 2001). Whether or not the non-linear terms can affect the large scale

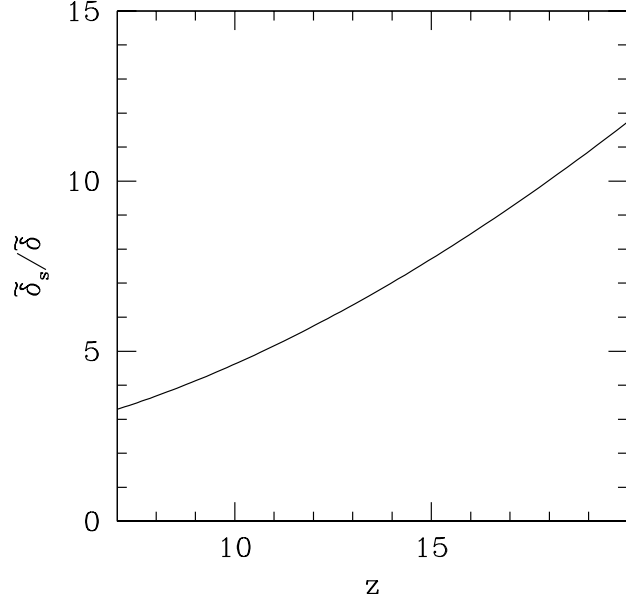


Figure 8. The evolution of the source bias $\tilde{\delta}_s/\bar{\delta} (= \tilde{\Delta}_s/(f_s\bar{\delta}))$ using eq.[32] and eq.[33].

At the end of reionization, our conclusion about the ionization topology may seem counter-intuitive, especially for X-ray reionizations. Assuming a homogeneous radiation background (which is the limiting case for very hard spectra of the X-ray reionization scenarios considered here), one finds that in the limit of a low neutral fraction, $x_{\text{HI}} \equiv n_{\text{HI}}/n_{\text{H}}$, ionization equilibrium implies $x_{\text{HI}} \propto n_{\text{H}}$, i.e. more overdense regions are less ionized. Therefore, the ionization topology should be “outside-in” rather than inside-out, in the limit of late times and a very hard spectrum. Our calculations above do not reveal this limiting case, however, for the following reasons: (i) our sources do not have arbitrarily hard spectra, (ii) we include a clustering of the ionizing sources, which, together with the rapid evolution of the emissivity, causes the background radiation to be persistently non-uniform. We have, however, checked that our code can reproduce the outside-in limiting case when we set the source bias to be zero (i.e. at late times, our code yields the expected behavior $\tilde{\delta}_{\text{HII}}/\bar{\delta} \sim (1 - \bar{x}_{\text{HI}}) < 1$, which follows from $x_{\text{HI}} \propto n_{\text{H}}$ in the limit of a small mean neutral fraction \bar{x}_{HI} and small fluctuations).

We have made at least two important simplifications in our calculations. One is ignoring helium. The other is to assume the source bias is deterministic.¹⁷ It is in principle

ionization topology is still an open question (although the arguments in Appendix B suggest that the high order effects can be neglected on sufficiently large scales).

¹⁷ In other words, we have assumed the source overdensity is linearly proportional to the local mass overdensity. The relation between the two is expected to be more complex in general: it could be stochastic and the sources certainly have Poisson fluctuations. In essence, we assume in this paper the stochasticity and Poisson fluctuations are negligible on the scales of interest.

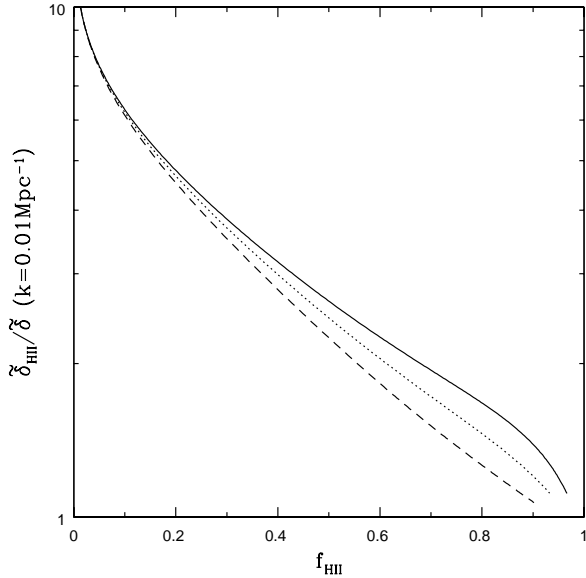


Figure 9. The bias of HII as a function of mean ionized fraction. The solid, dotted, and dashed curves correspond to energy cut-offs at 170eV, 270eV, and 450eV respectively, *i.e.* photons below this energy were erased for the $\beta = -1$ source spectrum.

straightforward to relax these assumptions/restrictions. We hope to do so in a future paper.

In practice, we still know little about the source properties at redshift above six. This work can serve as a link between the high redshift sources and the large scale distributions of the HII regions and the radiation fields. For example, as we have shown, the bias of the source distributions is similar to that of the HII regions during the early period of reionization; the evolution history of the bias of the HII regions can be used to constrain the hardness of the source spectrum. It allows us to constrain the source properties with the upcoming 21cm observations and the kinetic SZ effect from the CMB. Furthermore, as we have found in our calculation that the distribution of HII traces the dark matter's on large scales with a scale independent bias, these observations may also be used to measure the shape of the linear matter power spectrum. A more careful discussion of these issues will appear in another paper.

6 CONCLUSIONS

We have developed a perturbation theory of cosmic reionization by solving the linearized radiative transfer equation and the equation of ionization balance in Fourier space. The formalism can be used to predict the large scale fluctuations of the HII regions and the radiation fields for a given spatial distribution and spectrum of the ionizing sources. The numerical solutions are straightforward to obtain. In the case of UV dominated source spectra, we have found an approximate analytic solution which works accurately in the early stages of reionization.

To illustrate our formalism, we use the extended Press-

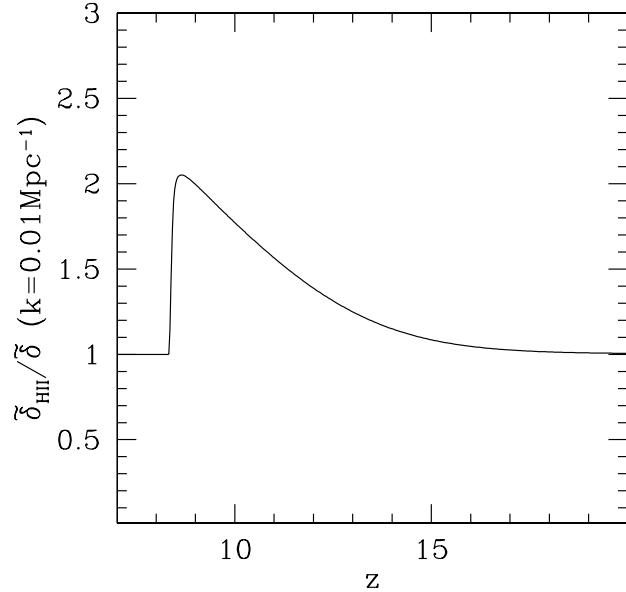


Figure 10. The bias of HII as a function of redshift in the model with $\beta = -3$ source spectrum, but assuming an unbiased source population.

Schechter theory to model the source clustering and adopt three different power-law type source spectra. We find that for UV dominated source spectra, the biases of the HII regions and the UV photons remain high during most of the reionization process. For hard source spectra, the HII regions tend to be ionized in a more homogeneous manner. The HII bias decays faster with time due to a longer photon mean free path and due to secondary ionization. The topology of the HII distribution is always inside-out, with overdense regions more highly ionized, at least on large scales.

Our findings suggest that clustering measurements from future 21cm and CMB observations can be used to put constraints on properties (both clustering and spectra) of the ionizing sources. Furthermore, on sufficiently large scales, both HII and HI have a scale independent bias with respect to dark matter – this means the same observations might be used to measure the shape of the matter power spectrum.

A direct comparison of our results with 3D simulations (such as those by Kohler et al. 2005, Iliev et al. 2005, and Zahn et al. 2006) would be valuable and interesting. An accurate comparison requires detailed information on the source properties and the clumping factors from the simulations, and we hope to perform such a comparison in a future paper.

ACKNOWLEDGEMENTS

We thank Greg Bryan, Steven Furlanetto, Ilian Iliev, Adam Lidz, and Jeremiah P. Ostriker for useful comments on an earlier version of this manuscript. Research for this work is supported in part by the DOE, grant number DE-FG02-92-ER40699. ZH acknowledges support by NASA through grants NNG04GI88G and NNG05GF14G, by NSF through

grants AST0307291, and by the Hungarian Ministry of Education through a György Békésy Fellowship.

REFERENCES

- Arons J. & Wingert D. 1972, *ApJ*, 177, 1
 Barkana R. & Loeb A., 2001, *Phys. Rep.*, 349, 125
 Baugh C., Cole S., Frenk C. & Lacey C., 1998, *ApJ*, 498, 504
 Becker R. et al., 2001, *AJ*, 122, 2850
 Benson A., Nusser A., Sugiyama N. & Lacey C., 2001, *MNRAS*, 320, 153
 Benson A., Lacey C., Baugh C., Cole S. & Frenk C., 2002, *MNRAS*, 333, 156
 Benson A., Sugiyama N., Nusser A. & Lacey C., 2005, *astro-ph/0512364*
 Bond J., Cole S., Efstathiou G. & Kaiser N., 1991, *ApJ*, 379, 440
 Bruscoli M., Ferrara A., Fabbri R. & Ciardi B., 2000, *MNRAS*, 318, 1068
 Chiu W. & Ostriker J., 2000, *ApJ*, 534, 507
 Chiu W., Fan X. & Ostriker J., 2003, *ApJ*, 599, 759
 Choudhury T. & Ferrara A., 2006, *astro-ph/0603149*
 Ciardi B., Ferrara A., Governato F. & Jenkins A., 2000, *MNRAS*, 314, 611
 Ciardi B., Ferrara A., Marri S. & Raimondo G., 2001, *MNRAS*, 324, 381
 Ciardi B., Stoehr F. & White S., 2003, *MNRAS*, 343, 1101
 Cole S., Lacey C., Baugh C. & Frenk C., 2000, *MNRAS*, 319, 168
 Dijkstra M., Haiman Z. & Scharf C., 2005, *ApJ*, 624, 85
 Dijkstra M., Haiman Z., Rees M. & Weinberg D., 2004, *ApJ*, 601, 666
 Djorgovski S., Castro S., Stern D. & Mahabal A., 2001, *ApJ*, 560, 5
 Fan X. et al., 2002, *AJ*, 123, 1247
 Fan X., Carilli C. & Keating B., 2006, *ARAA*, 44, 415
 Field G., 1958, *Proc. IRE*, 46, 240
 Field G., 1959, *ApJ*, 129, 525
 Furlanetto S., Zaldarriaga M. & Hernquist L., 2004, *ApJ*, 613, 1
 Gnedin N., 2000, *ApJ*, 535, 530
 Gnedin N., 2000, *ApJ*, 542, 535
 Gnedin N. & Hui L., 1998, *MNRAS*, 296, 44
 Gnedin N. & Ostriker J., 1997, *ApJ*, 486, 581
 Gruzinov A. & Hu W., 1998, *ApJ*, 508, 435
 Gunn J. & Peterson B., 1965, *ApJ*, 142, 1633
 Haiman Z., 2002, *ApJL*, 576, 1
 Haiman Z., Abel T. & Madau P., 2001, *ApJ*, 551, 599
 Haiman Z. & Cen, R., 2005, *ApJ*, 623, 627
 Haiman Z. & Holder G., 2003, *ApJ*, 595, 1
 Haiman Z. & Loeb A., 1997, *ApJ*, 483, 21
 Haiman Z. & Spaans M., 1999, *ApJ*, 518, 138
 Hui L., Haiman Z., 2003, *ApJ*, 596, 9
 Hui L., Gnedin N., 1997, *MNRAS*, 292, 27
 Hui L., Seljak U., 1996, *Proceedings of the 173rd Symposium of the IAU*, edited by Kochanek C. S. and Hewitt J. N., Kluwer Academic Publishers
 Iliev I., Mellema G., Pen U., Merz H., Shapiro P. & Alvarez M., 2005, *astro-ph/0512187*
 Iliev I., Scannapieco E. & Shapiro P., 2005, *ApJ*, 624, 491
 Iliev I., Pen U., Bond J., Mellema G. & Shapiro P., 2006, *astro-ph/0607209*
 Kaplinghat M., Chu M., Haiman Z., Holder G., Knox L., Skordis C., 2003, *ApJ*, 583, 24
 Knox L., Scoccimarro R. & Dodelson S., 1998, *PRL*, 81, 2004
 Kogut A. et al., 2003, *ApJS*, 148, 161
 Kohler K., Gnedin N. & Hamilton A., 2005, *astro-ph/0511627*
 Kolb E. W., Matarrese S. & Riotto A., 2005, *astro-ph/0506534*
 Kramer R., Haiman Z. & Oh S., 2006, *astro-ph/0604218*
 Lacey C. & Cole S., 1993, *MNRAS*, 262, 627
 Madau P., Meiksin A. & Rees M., 1997, *ApJ*, 475, 429
 Mellema G., Iliev I., Pen U. & Shapiro P., 2006, *astro-ph/0603518*
 Mesinger A., Bryan G. & Haiman Z., 2006, *astro-ph/0604148*
 Miralda-Escudé J., Haehnelt M. & Rees M., 2000, *ApJ*, 530, 1
 Oh S., 2001, *ApJ*, 553, 499
 Oh S. & Haiman Z., 2003, *MNRAS*, 346, 456
 Osterbrock D. E., Ferland G. J., 2005, *Astrophysics of Gaseous Nebulae and Active Galactic Nuclei* (University Science Books)
 Page L., Hinshaw G., Komatsu E., Nolta M., Spergel D., Bennett C., Barnes C., Bean R., Dore' O., Halpern M., Hill R., Jarosik N., Kogut A., Limon M., Meyer S., Odegard N., Peiris H., Tucker G., Verde L., Weiland J., Wollack E., Wright E., 2006, *astro-ph/0603449*
 Peebles P., 1980, *Large-Scale Structure of the Universe* (Princeton University Press)
 Press W. & Schechter P., 1974, *ApJ*, 187, 425
 Malhotra, S., Rhoads J. E., 2004, *ApJL*, 617, 5
 Ricotti M. & Ostriker J., 2004, *MNRAS*, 352, 547
 Salvaterra R., Ciardi B., Ferrara A. & Baccigalupi C., 2005, *MNRAS*, 360, 1055
 Santos M. et al., 2003, *ApJ*, 598, 756
 Santos M. et al., 2004, *ApJ*, 606, 683
 Scott D. & Rees M., 1990, *MNRAS*, 247, 510
 Sokasian A., Abel T., Hernquist L. & Springel V., 2003, *MNRAS*, 344, 607
 Sokasian A., Yoshida N., Abel T., Hernquist L. & Springel V., 2003, *MNRAS*, 350, 47
 Spergel D. et al., 2003, *ApJS*, 148, 175
 Spergel D., Bean R., Dore' O., Nolta M., Bennett C., Hinshaw G., Jarosik N., Komatsu E., Page L., Peiris H., Verde L., Barnes C., Halpern M., Hill R., Kogut A., Limon M., Meyer S., Odegard N., Tucker G., Weiland J., Wollack E., Wright E., 2006, *astro-ph/0603449*
 Shull J. & Van Steenberg M., 1985, *ApJ*, 298, 268
 Sunyaev R. & Zel'dovich I., 1980, *MNRAS*, 190, 413
 Theuns T., Schaye J., Zaroubi S., Kim T.-S., Tzanavaris P., Carswell B. 2002, *ApJL*, 567, 103
 Valageas P., Balbi A. & Silk J., 2001, *A&A*, 367, 1
 Valageas P. & Silk J., 1999, *A&A*, 347, 1
 Venkatesan, A., Giroux, M. L., & Shull, J. M. 2001, *ApJ*, 563, 1
 White R., Becker R., Fan X. & Strauss M., 2003, *AJ*, 126, 1
 Wyithe J. & Loeb A., 2004, *Nature*, 427, 815
 Zahn O., Lidz A., Mcquinn M., Dutta S., Hernquist L., Zal-

darriaga M., Furlanetto S., 2006, astro-ph/0604177
 Zaldarriaga M., 1997, PRD, 55, 1822
 Zaldarriaga M., Furlanetto S. & Hernquist L., 2004, ApJ,
 608, 622

APPENDIX A – ANALYTIC SOLUTIONS TO THE FIRST ORDER RADIATIVE TRANSFER AND IONIZATION EQUATIONS

Use eq.[24] in eq.[20], we find the following equation for $\tilde{\Delta}_{HII}$:

$$\frac{\partial \tilde{\Delta}_{HII}}{\partial \omega} = \tilde{\delta}_{eff} - F \tilde{\Delta}_{HII} + \int_{-\infty}^{\omega} d\omega' K(\omega, \omega') \tilde{\Delta}_{HII}(\omega') \quad (38)$$

where

$$\begin{aligned} K(\omega, \omega') &= 4\pi \frac{\sin[P(\omega, \omega')k]}{P(\omega, \omega')k} \\ &\times \int_0^{\infty} d\mu B(\omega, \mu) \langle \kappa(\mu) \rangle R(\omega', \mu + \omega - \omega') \\ &\times \exp\left[-\int_{\omega'}^{\omega} d\omega'' B(\omega'', \mu + \omega - \omega'')\right] \end{aligned} \quad (39)$$

and

$$\begin{aligned} \tilde{\delta}_{eff}(\omega) &= G(\omega) \tilde{\delta}(\omega) - \int_{-\infty}^{\omega} d\omega' K(\omega, \omega') \tilde{\delta}(\omega') \\ &+ 4\pi \int_{-\infty}^{\omega} d\omega' \frac{\sin[P(\omega, \omega')k]}{P(\omega, \omega')k} N(\omega') \\ &\times \int_0^{\infty} d\mu B(\omega, \mu) \langle \kappa(\mu) \rangle \tilde{\Delta}_s(\omega', \mu + \omega - \omega') \\ &\times \exp\left[-\int_{\omega'}^{\omega} d\omega'' B(\omega'', \mu + \omega - \omega'')\right] \end{aligned} \quad (40)$$

To solve eq.[38], we use an integrating factor $\theta(\omega)$ which is defined as:

$$\frac{d\theta}{d\omega} = \theta(\omega) F(\omega) \quad (41)$$

and multiply both sides of eq.[38] by $\theta(\omega)$:

$$\frac{\partial(\theta \tilde{\Delta}_{HII})}{\partial \omega} = \theta \tilde{\delta}_{eff} + \theta \int_{-\infty}^{\omega} d\omega' K(\omega, \omega') \tilde{\Delta}_{HII}(\omega') \quad (42)$$

or

$$\begin{aligned} \frac{\partial(\theta \tilde{\Delta}_{HII})}{\theta \partial \omega} &= \tilde{\delta}_{eff} + \int_{-\infty}^{\omega} d\omega' K(\omega, \omega') \\ &\times \theta^{-1}(\omega') \int_{-\infty}^{\omega'} d\omega'' \frac{\partial(\theta \tilde{\Delta}_{HII})}{\partial \omega''} \end{aligned} \quad (43)$$

Defining the function $f(\omega)$:

$$f(\omega) = \frac{\partial(\theta \tilde{\Delta}_{HII})}{\theta \partial \omega} \quad (44)$$

and changing the order of the integration, we can re-write eq.[43] as:

$$f(\omega) = \tilde{\delta}_{eff}(\omega) + \int_{-\infty}^{\omega} d\omega' T(\omega, \omega') f(\omega') \quad (45)$$

where

$$T(\omega, \omega') = \int_{\omega'}^{\omega} d\omega'' K(\omega, \omega'') \frac{\theta(\omega')}{\theta(\omega'')} \quad (46)$$

Eq.[45] is a standard Volterra integral equation of the second kind. Its solution can be easily generated by inverting a triangular matrix. Using $f(\omega)$, it is not hard to calculate $\tilde{\Delta}_{HII}$. One can then use eq.[23] to get $\tilde{\Delta}_\gamma$ or eq.[24] to get the monopole of $\tilde{\Delta}_\gamma$.

APPENDIX B – ON THE VALIDITY OF LINEAR PERTURBATION THEORY

In this Appendix, we address the following question: is linear perturbation theory justified on large scales even when highly nonlinear structures exist on small scales? This is a deep question that arises both in the present context of reionization and in the more familiar context of large scale structure formation theory. We will make no attempt to provide a rigorous justification here. Instead, we will make some plausibility arguments, which are borrowed from the field of large scale structure (Peebles 1980). Ultimately, numerical simulations are needed to rigorously justify the use of perturbation theory on large scales.

The fundamental equations are eq.[3] for ionization balance and eq.[4] for radiative transfer. If the right hand sides of these equations were zero, these equations simply express conservation for n_{HII} and n_γ . If this were to hold true, we expect perturbation theory to work on large scales just like it is known to do for large scale structure – similar conservation equations appear in large scale structure. Let us instead focus on the right hand sides which contain the novel aspects of the reionization problem. Morally one can think of eq.[3] as :

$$\frac{dn_{HII}}{d\tau} = \text{ionization} - \text{recombination} \quad (47)$$

and one can think of eq. [4] as:

$$\frac{dn_\gamma}{d\tau} = \text{source} - \text{sink} \quad (48)$$

The 'ionization', 'recombination' and 'sink' terms all contain quadratic combinations of the dynamical variables and are potentially what could cause the break down of perturbation theory. Let us divide space into regions where perturbations are large and where they are small. We will refer to these as the 'linear' and 'nonlinear' regions. Taking Fourier transform of the equation for ionization balance, we have

$$\begin{aligned} \int d^3x \frac{dn_{HII}}{d\tau} e^{i\vec{k}\cdot\vec{x}} &= \\ \int_{\text{linear}} d^3x [\text{ionization} - \text{recombination}] e^{i\vec{k}\cdot\vec{x}} &+ \\ \int_{\text{nonlinear}} d^3x [\text{ionization} - \text{recombination}] e^{i\vec{k}\cdot\vec{x}} \end{aligned} \quad (49)$$

The linear regions are simple to deal with: we can linearize the 'ionization' and 'recombination' terms. The nonlinear regions potentially could give large contributions, but here we make use of a key insight: such regions are often in ionization equilibrium (i.e. 'ionization' roughly balances 'recombination') making the nonlinear contributions actually quite small. A very similar argument is used in the context of large

scale structure, where one invokes virial equilibrium as opposed to ionization equilibrium to argue for the cancelation of potentially large terms. What are these nonlinear regions in our case? They could be HII bubbles at the beginning of reionization, or self-shielded Lyman-limit systems at the end of reionization, for instance.

Setting the last term of eq.[49] to be zero, we have

$$\int d^3x \frac{dn_{HII}}{d\tau} e^{i\vec{k}\cdot\vec{x}} = \int d^3x W(\vec{x}) [\text{ionization} - \text{recombination}]_{\text{linear}} e^{i\vec{k}\cdot\vec{x}} \quad (50)$$

where we have introduced a mask $W(x)$ which vanishes in the nonlinear regions, and equals unity in the linear regions, and we have linearized the ionization and recombination terms.

Ultimately, we are interested in the power spectrum of fluctuations in n_{HII} for instance. Eq.(50) tells us that its evolution can be regarded as linear as long as we are studying scales k on which the mask W , or its Fourier transform, has a negligible effect on the power spectrum. Generally, the linear approximations will be valid only on scales much larger than the size of the nonlinear regions, and likely even larger than the clustering scale of the nonlinear regions. For instance, in the early stages of reionization, we expect perturbation theory to work only on scales that encompass many HII bubbles. Note that the mask in question is more complex than the usual masks in galaxy surveys: here, the mask is correlated with the signal in non-trivial ways, and it is by no means obvious that the large scale power spectrum is unaffected by such masking. Addressing this important issue is beyond the scope of this paper.

How about the radiative transfer equation? Applying a similar split, we have

$$\int d^3x \frac{dn_\gamma}{d\tau} e^{i\vec{k}\cdot\vec{x}} = \int_{\text{linear}} d^3x [\text{source} - \text{sink}] e^{i\vec{k}\cdot\vec{x}} + \int_{\text{nonlinear}} d^3x [\text{source} - \text{sink}] e^{i\vec{k}\cdot\vec{x}} \quad (51)$$

Here, the situation is similar to the ionization balance equation, in that in nonlinear regions, one expect the 'source' and 'sink' to roughly cancel, but in general, we don't expect exact cancelation. For instance, one can think of a galaxy where the UV photons are propagating out of a thick medium. Most of the photons are consumed within the galaxy, but inevitably there will be some that escape. One usually quantifies this by the escape fraction. Here, we can account for this effect by renormalizing the source:

$$\int d^3x \frac{dn_\gamma}{d\tau} e^{i\vec{k}\cdot\vec{x}} = \int d^3x [\text{source}_{\text{renorm.}} - W(\vec{x}) \text{sink}] e^{i\vec{k}\cdot\vec{x}} \quad (52)$$

The mask W is the same as before, and the 'sink' term can be linearized. The 'source' term can be thought of as a new effective source that accounts for the escape fraction from the nonlinear regions.